

# BrightMarker: 3D Printed Fluorescent Markers for Object Tracking

Mustafa Doga Dogan  
MIT CSAIL  
Cambridge, MA, US  
doga@mit.edu

Jamison John O'Keefe  
MIT CSAIL  
Cambridge, MA, US  
jjokeefe@mit.edu

Raul Sanchez-Reillo  
Universidad Carlos III de Madrid  
Leganes, Madrid, Spain  
raul.reillo@uc3m.es

Raul Garcia-Martin  
MIT CSAIL  
Cambridge, MA, US  
raulg@mit.edu

Ahmad Taka  
MIT CSAIL  
Cambridge, MA, US  
ahmadtak@mit.edu

Stefanie Mueller  
MIT CSAIL  
Cambridge, MA, US  
stefanie.mueller@mit.edu

Patrick William Haertel  
MIT CSAIL  
Cambridge, MA, US  
phaertel@mit.edu

Akarsh Aurora  
MIT CSAIL  
Cambridge, MA, US  
aaurora@mit.edu



Figure 1: BrightMarkers are embedded into objects using a NIR-fluorescent filament. (a) When viewed with a NIR camera with the matching filter, the markers appear with high contrast, which allows them to be tracked even when the objects are in motion, e.g., on a conveyor belt. (b) BrightMarker can be used to fabricate custom wearables for tracking, or (c) for transforming physical controls into precise input methods in mixed reality environments.

## ABSTRACT

Existing invisible object tagging methods are prone to low resolution, which impedes tracking performance. We present BrightMarker, a fabrication method that uses fluorescent filaments to embed easily trackable markers in 3D printed color objects. By using an infrared-fluorescent filament that "shifts" the wavelength of the incident light, our optical detection setup filters out all the noise to only have the markers present in the infrared camera image. The high contrast of the markers allows us to track them robustly regardless of the moving objects' surface color.

We built a software interface for automatically embedding these markers for the input object geometry, and hardware modules that can be attached to existing mobile devices and AR/VR headsets. Our image processing pipeline robustly localizes the markers in real time from the captured images.

BrightMarker can be used in a variety of applications, such as custom fabricated wearables for motion capture, tangible interfaces for AR/VR, rapid product tracking, and privacy-preserving night vision. BrightMarker exceeds the detection rate of state-of-the-art invisible marking, and even small markers (1"x1") can be tracked at distances exceeding 2m.

## CCS CONCEPTS

- Human-centered computing → Human computer interaction (HCI).

## KEYWORDS

3D printing; digital fabrication; fluorescence; infrared imaging; marker tracking; invisible markers

## ACM Reference Format:

Mustafa Doga Dogan, Raul Garcia-Martin, Patrick William Haertel, Jamison John O'Keefe, Ahmad Taka, Akarsh Aurora, Raul Sanchez-Reillo, and Stefanie Mueller. 2023. BrightMarker: 3D Printed Fluorescent Markers for Object Tracking. In *The 36th Annual ACM Symposium on User Interface Software and Technology (UIST '23)*, October 29–November 01, 2023, San Francisco, CA, USA. ACM, New York, NY, USA, 13 pages. <https://doi.org/10.1145/3586183.3606758>



This work is licensed under a Creative Commons Attribution-NonCommercial-ShareAlike International 4.0 License.

UIST '23, October 29–November 01, 2023, San Francisco, CA, USA

© 2023 Copyright held by the owner/author(s).

ACM ISBN 979-8-4007-0132-0/23/10.

<https://doi.org/10.1145/3586183.3606758>

## 1 INTRODUCTION

Tags and markers play a vital role in interactions with objects in human-computer interaction (HCI). The ability to identify and track objects in real time enables a wide range of applications, such as motion capture for animation and gaming [7, 66], augmented and virtual reality (AR/VR) [2, 52], and object tracking for industrial and robotic applications [16, 59].

In recent years, the need for invisible object tagging has become increasingly important. The ability to track objects without the markers having a bulky form factor or being in the user's direct view allows for a more natural and immersive experience for users, and opens up new possibilities for tracking objects in real-life scenarios where visible markers would be impractical and obtrusive.

However, existing methods for invisible object tagging have several limitations that impede their widespread adoption. One significant limitation is their low signal-to-noise (SNR) ratio, i.e., the poor resolution and clarity of the imaged marker. Because invisible markers are embedded in the interior of objects, the markers are imaged from a weak signal, which needs to be amplified by optical and digital processes [30, 64]. These processes result in long capture or decoding times, typically ranging from seconds to minutes per frame. This deteriorates further when objects are in motion, i.e., the captured markers appear blurrier and are thus unidentified in most frames. In addition, existing invisible tags are often limited in terms of the variety of object colors they can be used with. For example, *InfraredTags* [13] embedded 3D printed codes in black objects, and *AirCode* [30] in white objects.

To address these limitations, we present *BrightMarker*, a fabrication method for passive invisible tags using fluorescent filaments that emit light in a specific near-infrared (NIR) wavelength, which NIR cameras can robustly detect. By isolating the markers from the rest of the scene using the matching filter, we are able to robustly track markers even when objects are in motion. Our work builds on *InfraredTags* and addresses the limitations in regard to marker resolution and object colors by enhancing detection. We were inspired by the motion capture system *OptiTrack*, which uses passive retro-reflective markers that reflect the shined IR to the camera.

We demonstrate the potential of *BrightMarker* by showcasing various applications, including product tracking on conveyor belts, flexible wearables for motion capture, tangible and haptic interfaces for AR/VR, and privacy-preserving night vision. Our technical evaluation shows that the markers embedded in a variety of surface colors can be detected robustly and in real time as they move.

We believe that *BrightMarker* is a promising approach that could significantly improve the performance and versatility of invisible object tagging and have a wide range of potential HCI applications.

In summary, we make the following contributions:

- A novel method that uses fluorescent filaments and imaging to integrate invisible and passive tracking markers into 3D printed objects of different colors.
- A software interface that uniformly distributes markers onto 3D models based on their geometry.
- A detection hardware module for real-time fluorescence tracking that can be attached to existing AR/VR headsets.
- An image processing pipeline that allows real-time tracking of the integrated markers.

- The evaluation of the design space, including object colors, under various distance and lighting conditions.
- A demonstration of the potential applications of our approach, including custom-fabricated motion capture wearables, AR/VR tangibles, and privacy-preserving night vision.

## 2 RELATED WORK

In this section, we explain previous work on motion capture approaches, invisible marker systems in the fabrication literature, as well as the infrared-based materials used in these systems.

### 2.1 Motion Capture Systems

Motion capture, abbreviated as "mocap," describes the technologies used to capture, track, and digitize physical objects and humans in real time. Existing motion capture systems are typically based on *external* markers, i.e., a tracking marker needs to be separately attached to the objects that are intended to be tracked. Such markers are typically based on inertial or optical methods. Inertial systems use gyroscopes and accelerometers to measure the orientation and acceleration of objects (e.g., *Xsens* [46]). Optical methods use cameras to track markers mounted on objects and software to translate the marker positions into motion data.

Widely used optical systems, such as *OptiTrack* [20] and *Vicon* [36], offer active and passive optical markers that can be tracked by setting up multiple cameras in the environment. Active markers commonly include LEDs [38], which are picked up by these cameras, or sensors that detect the IR radiation emitted by nearby light sources. Such markers require an embedded power source and can be large compared to the object, (e.g., *Vive Tracker* [5] is >7cm in two dimensions). Passive markers, on the other hand, are beads coated with a retro-reflective material that reflects the light shined by the detection hardware [2]. Whether active or passive, optical methods require multiple cameras to be set up and calibrated to accurately track objects, which can be both time-consuming and costly (e.g., a 6-camera *OptiTrack* system costs >\$9k). Furthermore, given that these markers are external, they need to be attached to objects, which limits their use and practicality in real-world use.

*BrightMarker* aims to overcome these limitations by using embeddable fluorescent materials to create passive tracking markers that can be *integrated* into real-world objects and tracked using just one camera. This allows for more affordable, versatile, and unobtrusive tracking of objects in real-world applications without the need for manual and visible attachment of markers.

### 2.2 Integrated and Invisible Markers

To move away from *external* tracking markers that are manually attached to objects, researchers proposed *integrated* markers that can be an inherent part of objects using digital fabrication methods. 3D printing has been used for embedding markers into interactive objects that can sense touch, identity, or deformation [11, 31, 48]. For instance, *Capricate* [50] tracks users' touch on 3D printed objects using embedded conductive markers. *CapCodes* [25] and *BYO\** [26] take this further by allowing the identification of individual objects. *Flexibles* [51] can sense deformation of flexible tangibles on capacitive touchscreens. *3D-Auth* [32] uses 3D-printed patterns for user

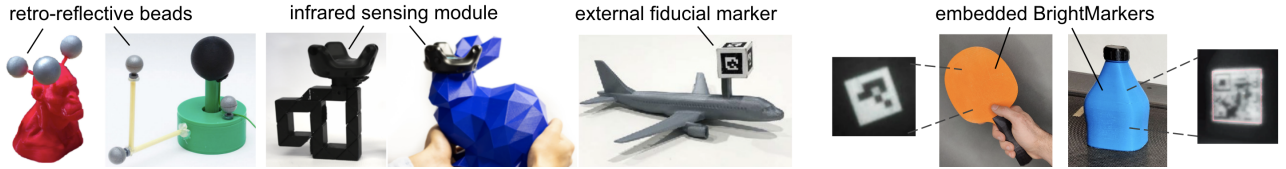


**Figure 2: Ways to add tracking capabilities to real-world objects as used in previous HCI projects.** External tags rely on adding retro-reflective beads [18, 52], sensor modules [17, 66], or fiducial markers [53], but may result in bulky or visually obtrusive objects. To address this, *BrightMarker* (rightmost) embeds high-contrast markers using a fluorescent material.

authentication, and *Off-Line Sensing* [49] uses 3D printed structures filled with liquids to verify one-time interactions such as flipping.

For tracking objects in 3D, researchers suggested integrating optical markers or fiducial markers that can be imaged using cameras. For example, *TrackItPipe* [52] allows users to automatically augment existing 3D printable models with stand-offs for inserting markers for optical systems such as *OptiTrack*. Fiducial markers, such as *ArUco* [41] and *AprilTags* [39], can be added to 3D printed objects [53, 54] and other existing physical objects to track and interact with them [45, 65]. In addition, the shapes of these markers can be customized for objects' surfaces to fit their outline [22].

Figure 2 shows several external tags used in previous HCI projects focused on bringing real-world objects into AR/VR and tangible applications. These tags rely on adding retro-reflective beads [18, 52], sensor modules [17, 66], or fiducial markers [53], but may result in bulky or visually obtrusive objects. This limits the object's real-world usability beyond its digital applications.

To address the bulkiness and visual obtrusiveness, researchers utilized various imaging methods to achieve integrated tags that are truly *invisible*. *AirCode* [30] uses a projector-based computational method, and *InfraStructs* [64] uses terahertz scanners to embed markers, which need a decoding time on the order of minutes per frame. Methods such as *InfraredTags* [13, 14] and *interiqr* [37] use specific materials such as infrared-translucent filaments or dough, which can be imaged faster using regular infrared cameras. However, all of these methods are prone to motion blur and thus not suitable for real-time tracking. Further, they are limited in the material/color options that objects may have.

### 2.3 Infrared-Based and Fluorescent Materials

Infrared (IR) based methods have become a popular choice for embedding markers invisibly. Different material properties have been employed to embed patterns, including IR reflection, translucency, and absorption. For example, *MiniStudio* [29] uses screen printing to apply IR-reflective stickers with fiducial markers, while *InfraredTags* [13] makes markers imperceptible by covering them with an opaque, IR-passing material. On the other hand, *Spyn* [42] adds IR-absorbing inks into knitted objects and *HideOut* [63] creates hidden tracking markers by using IR-absorbing ink, although a spray gun is required for the latter. *DeforMe* [40] computes the deformation of elastic materials by tracking dots painted with IR-absorbing ink. *StandARone* [12] applies the ink using inkjet printers to rapidly add AR watermarks to paper documents.

Despite their wide use in several fields such as imaging [57], lighting [28], medicine [55], and forensics [35], fluorescence has

not been widely explored in personal fabrication research. Material scientists recently developed resins that can be used for 3D printing fluorescent materials [21, 44]. Today there are commercial fused deposition modeling (FDM) filaments available that glow when exposed to UV light [33, 34], however, these fluoresce light in the visible wavelength range, which is unsuitable for embedding *invisible* markers.

In this work, we leverage a 3D printing filament developed by *DIC Corporation* [8] and *Silapasuphakornwong et al.* [56] for the purpose of embedded and passive object tracking. We use this filament since it is ABS-based, which can be readily employed with accessible FDM printers and emits light in the NIR range, allowing the markers to remain hidden from end users. Compared to the past prototype [56], we are interested in the in-depth analysis and scientific explanation of fluorescence-based tagging for real-time tracking. Our goal is to optimize and evaluate the tracking process for various object colors and marker types, and to develop insights and tools to help researchers and practitioners in the field.

Our proposed method, *BrightMarker*, enables the invisible integration of real-time tracking markers by incorporating IR-fluorescent materials during the 3D printing of physical objects. By using fluorescent filaments that emit light in a specific wavelength, we filter out all the non-desired illumination to have solely the fluorescent markers present in the IR camera image. This allows us to track markers robustly even when objects are in motion.

## 3 BRIGHTMARKER: HIGH-CONTRAST MARKERS USING FLUORESCENT FILAMENTS

*BrightMarker* has the benefit of using fluorescent filaments, which allow us to achieve high marker contrast in the filtered infrared images. Fluorescence is the physical phenomenon in which a material *absorbs* light at one wavelength and *emits* it at a longer wavelength [24]. This occurs when a molecule absorbs the energy of light and temporarily enters an excited state, before releasing the energy as a lower-energy photon. The difference between these two wavelengths is called Stokes shift [43]. By shifting the illumination from shorter wavelengths to longer ones, the fluorescent color can appear more saturated than it would by reflection alone, which enhances its detectability [47]. For this reason, fluorescent materials are particularly useful for imaging and sensing applications.

In this work, we utilize fluorescence as a material property to create objects with easily trackable markers via multi-material 3D printing. The key material we use is a fluorescent 3D printing filament which contains uniformly distributed fluorescent dye. The

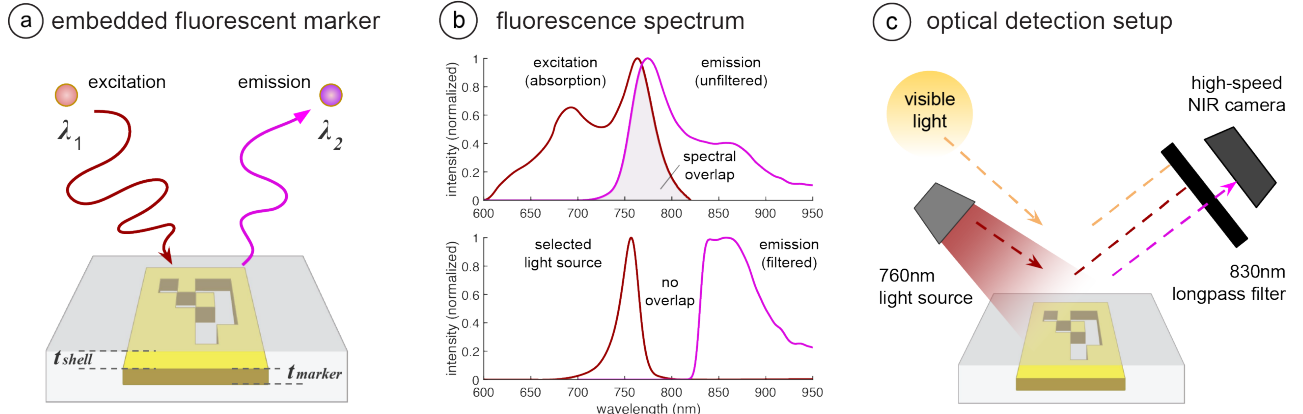


**Figure 3: Fluorescence and our imaging approach.** (a) *BrightMarker* embeds tracking markers with fluorescent filaments, which "shift" the wavelength of IR radiation. (b) Although the excitation and emission spectra of the filament overlap (top), they can be separated in practice using optical tools (bottom). (c) Our imaging setup filters for the marker's fluorescence.

filament emits light in a specific wavelength when excited by an IR light source. By using an optical filter of the appropriate wavelength for the camera, we are able to capture exclusively the light emitted by the filament and thus the parts fabricated from it.

### 3.1 Fluorescent Filament

We utilize an ABS (acrylonitrile butadiene styrene) filament developed by *DIC Corporation* [8] and Silapasuphakornwong et al. [56]. This filament contains a NIR-fluorescent dye, which reacts to the NIR light source by fluorescing as explained earlier. The fluoresced light can penetrate the exterior material of the object and thus be captured from the outside (Figure 3a).

**Fluorescence behavior:** To understand the fluorescence characteristics of this material and optimize our system for it, we measured its excitation and reaction using a fluorimeter (*HORIBA Jobin Yvon Fluorolog-3*). The top graph in Figure 3b shows both the *excitation* (absorption, plotted in red) and *emission* (fluorescence, plotted in purple) spectra of the material. As can be seen in these unfiltered spectra, the emitted fluorescence has a longer wavelength than the absorbed light: While the material is most excited at wavelength 763nm, the peak of the emitted light is at 775nm. This Stokes shift of 12nm between the two spectra allows us to separate the excitation and emission signals for the IR image capture. However, due to the spectral overlap highlighted in the graph, the excitation and emission signals first need to be filtered using optical methods, which we explain in the imaging section.

**Multi-material 3D printing:** The NIR-fluorescent filament is used in one of the print heads of a multi-material FDM printer. We used *Ultimaker 3* and *S5* for our prints. The printing method builds on *InfraredTags'* multi-material printing approach in terms of the high-level CAD modifications. When embedding a *BrightMarker*, however, the main object geometry is printed using the filament of the user's choice, while the fluorescent filament is used to print the marker placed in the interior of the object (Figure 3a). Because

the fluorescent filament's main polymer is ABS, it can be printed at standard ABS printing temperatures ( $\sim 250^\circ\text{C}$ ).

As shown in the cross-section in Figure 3a, we denote the thickness of the marker by  $t_{\text{marker}}$ , and the shell between the marker and the object surface by  $t_{\text{shell}}$ . If  $t_{\text{marker}}$  is too small, the fluorescence will be weak for robust marker capture. We found that one printed layer of the filament, i.e.,  $t_{\text{marker}} = 0.15\text{mm}$ , is sufficient for our applications. On the other hand, the value of  $t_{\text{shell}}$  depends on the material used for the main object geometry, which we explain next.

**Main object material and color:** Compared to *InfraredTags* [13] which only allows embedding into black objects, *BrightMarker* is compatible with multiple color options for the main object geometry (including object surface). Due to the high intensity of the fluoresced light, the emitted light can penetrate the shell above the fluorescent marker and reach the camera's image sensor.

We observed that the fluorescent marker can be combined with both PLA and ABS materials. This makes it possible to have a variety of colors for our fabricated objects. Since the fluorescent filament is ABS, we strive to use ABS for the main object geometry when possible, as it ensures similar printing parameters (e.g., temperature) among the two parts. The only ABS color we determined that does not pass the fluoresced light is black. This is because the carbon black used in the conventional filament absorbs most wavelengths [4]. Thus, for producing black objects, we use the IR-PLA filament [1] used in *InfraredTags*, which passes IR light.

Figure 4 shows the design space of material colors. As shown in the NIR camera images, a fluorescent checkerboard pattern is embedded in each test slab to determine  $t_{\text{shell}}$  for the different colors. The pattern is covered with increasing shell thickness, from  $t_{\text{shell}} = 0\text{mm}$  to  $t_{\text{shell}} = 3\text{mm}$ , thus the pattern contrast in the camera images gradually decreases. We choose  $t_{\text{shell}}$  such that at this value, the pattern is no longer in the visible camera image, i.e., its contrast is less than 5% [3]. Further, if the shell is too thin, this can result in a poor surface finish, as observed in the lower end of the slabs.

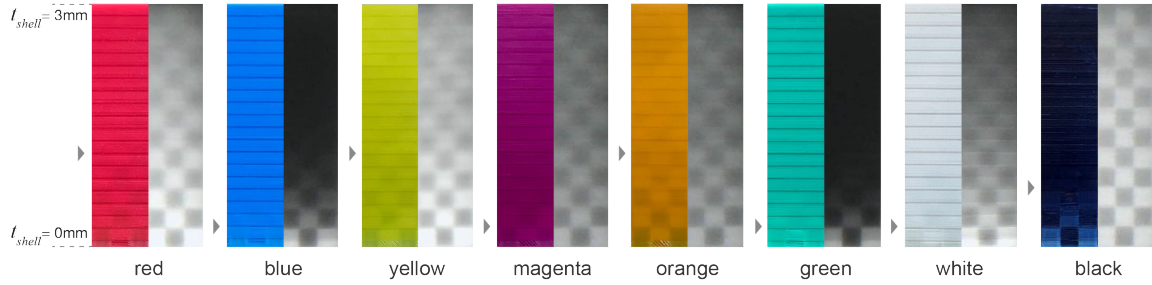


**Figure 4: The design space of possible material colors.** Each test slab was printed increasing shell thickness. The left image of each pair shows the visible camera capture, while the right image shows the NIR capture.

We found that colors closer to infrared, i.e., red, yellow, and orange, tend to be less opaque than other colors due to their dye composition. Thus, we use  $t_{shell} = 1.2\text{mm}$  for these colors. For other colors printed with ABS, we use  $t_{shell}=0.3\text{mm}$ . For the IR-PLA (rightmost), we use  $t_{shell}=0.8\text{mm}$ , which has a tinted appearance due to its translucent property. These values are marked in the figure with a small triangle to the left of the slabs. Larger thicknesses are also possible, but to ensure the detectability of the markers in IR, we recommend using values that maintain the bit binarization accuracy above 90% [13].

We note that these values also depend on the specific filament vendor and that variations might exist even among different batches from the same vendor. Thus, users are recommended to determine the optimal values for their filaments by first printing test slabs as illustrated in this section.

### 3.2 Infrared Imaging of Fluorescence

When coupled with wavelength-specific optical components, the light emitted by the fluorescent filament results in high contrast between the marker and the rest of the IR image. This allows us to robustly detect and track the objects in which the markers are embedded.

Our imaging system consists of three key components: (1) a light source for exciting the marker, (2) an optical filter for isolating marker fluorescence, and (3) a high-speed infrared camera. We explain the role of these components in the next sections.

**Light source for excitation:** Excitation of the NIR fluorescent material within the 3D printed object is necessary to read the embedded pattern. There are two considerations that an appropriate light source should meet for this purpose. First, the light emitted by the light source should be invisible to the user, i.e., there should be no emission below 700nm. Second, the light should excite the fluorescent material as much as possible. To achieve this, the light source should have high power, and its peak wavelength should be as close to the material's peak excitation wavelength (i.e., 763nm as explained in Section 3.1) as possible.

To satisfy these criteria in practice, we use LEDs that peak at 760nm and deliver high power. The bottom graph in Figure 3b shows the spectrum of the LED used in our high-speed imaging module (Section 4.2), marked red and labeled "selected light source." We note that the intensity reaches zero at approximately 800nm.

**Optical filter for marker isolation:** Through a wavelength-specific filter, we can enhance the recognition of fluorescent markers by minimizing interference from other wavelengths.

Due to the natural characteristics of fluorescence, there is an overlap between the higher wavelength end of the excitation spectrum and the lower wavelength end of the emission spectrum. This overlap, which is shown in the top graph of Figure 3b, must be eliminated to avoid overwhelming the weaker emitted fluorescence light with the brighter excitation light, which would significantly reduce marker contrast.

To separate these signals, we use a longpass filter with a cut-on wavelength of 830nm, which blocks any wavelength under this value from entering the camera. As shown in Figure 3c, it blocks the excitation light emitted by the LED (marked red) and the visible environmental light (marked yellow) from reaching the camera. The only wavelength range that can enter the camera corresponds to the fluorescence from the marker itself (marked purple). Therefore, as shown in the top graph of Figure 3b, there is no longer an overlap between the excitation and emission spectra: Our selected light source cuts the emission at ~810nm, while the filtered fluorescence that enters the camera starts at ~820nm. This separation allows the high intensity of the markers in captured images.

**High-speed NIR camera:** A high-speed camera allows the observation of the fluorescence emitted from the moving objects.

To capture images at a high frame rate and minimize motion blur, we use a 60-frames-per-second (fps) monochrome camera with a global shutter rather than a rolling shutter. Rolling shutters, which are commonly used in consumer-grade cameras, scan the image sensor line by line from top to bottom, resulting in a time delay between the capture of each row [23]. This can lead to motion blur in fast-moving scenes, which makes it difficult to detect the *BrightMarker* accurately.

In contrast, a global shutter captures the entire image simultaneously, resulting in no time delay between rows. This is crucial for real-time tracking where every frame counts. Additionally, a monochrome camera achieves higher spatial resolution than color cameras, and eliminates the need for a color filter array, which reduces the amount of light reaching the image sensor and decreases the camera's sensitivity to NIR fluorescence [62].

Together, these properties allow us to create a real-time video representation of the object with high temporal resolution.

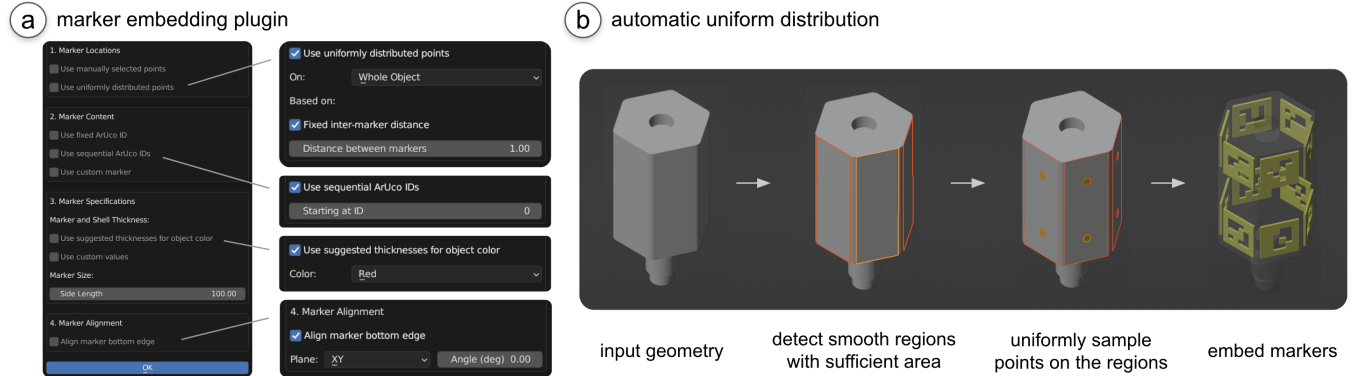


**Figure 5: Marker embedding process. (a) Our tool allows users to (b) uniformly distribute markers based on the object geometry.**

## 4 FABRICATING, CAPTURING, AND TRACKING BRIGHTMARKERS

In this section, we first describe the workflow in which *BrightMarkers* are added to objects for fabrication. We then explain the hardware and software we use for their detection once printed.

### 4.1 Adding Markers for Fabrication

Users start by importing a 3D model into the CAD editor (*Blender*). Next, the user specifies how the fluorescent marker(s) should be implanted using our plugin, which offers a variety of options as shown in Figure 5a.

**Determining marker locations:** In tracking applications, it is important to pad the object surface with numerous markers, rather than a single one, to ensure the object can be tracked independently of the object orientation. The user can either manually pick exact target points on the object for the marker embedding, or use an automatic distribution mode. This mode uniformly distributes points on the object geometry based on a fixed inter-marker distance or a total number of desired markers. The user can specify whether the target points should be distributed on the whole object, the areas other than the base, or a specific area selected by the user.

**Determining marker content:** The plugin allows users to embed ArUco markers with the same ID ("Use fixed ArUco ID") or increasing IDs ("Use sequential ArUco IDs") based on the desired use case. Unique sequential IDs can help identify an object's location and orientation. It is also possible to load a custom marker, such as a QR code or a Micro QR code, by selecting an image file.

**Determining marker depth and dimensions:** Next, the user specifies how deep the marker should be embedded under the object's surface. For this, the user can enter a custom value or simply select the desired object color from a dropdown, after which the plugin automatically retrieves the corresponding  $t_{shell}$  value from Section 3.1. Next the user can specify the dimensions of the marker. The marker thickness is set to the recommended  $t_{marker}$  value by default, and the user can specify a desired side length of the marker.

Finally, the user can specify whether the marker's bottom edge should be parallel to a certain plane. This helps users to align codes

in the 3D printing direction, which can lower print time and avoid print failures that might occur due to frequent nozzle switching. After setting up the parameters, users can start the embedding by clicking "OK". Once the markers are embedded, users can export the resulting STL files for 3D printing.

**3D printing:** The user imports the resulting STL files into the slicer software of the printer. For the popular slicer *Cura*<sup>1</sup>, we recommend disabling the "combing" parameter to ensure that the printer does not move over the already extruded pieces of fluorescent filament. This prevents the fluorescent filament from getting mixed into the outer surface layers and thus becoming visible.

**Implementation:** The automatic uniform distribution of the markers is created by first determining the areas on the model that are large enough and close to being flat to accommodate a marker of the user's specified size. This is done by comparing the angles between the normals of adjacent faces with the method `faces_select_linked_flat()`, grouping the ones with an angle difference smaller than 0.1 rad, and ensuring that the contained surface area is greater than that of the marker. This threshold can be adjusted based on the user's preference and application if desired. As shown in Figure 5b for the lightsaber model from Section 5.3, this gives the subregions on the object geometry that are not too curvy or sharp.

Next, to uniformly sample points, each subregion is temporarily duplicated, flattened, and its shape is approximated to a high degree of accuracy in an array of 1s and 0s created with repeated calls of the function `ray_cast()`. The array is analyzed row by row, choosing rows that are a distance of half the marker side length apart. Points in each row are picked if they are sufficiently far from each other and the edges of the subregion. Finally, using the specifications set by the user, a knife projection is used to project the marker so it has the same curvature as the object at the sampled point. The projected marker is extruded to form a 3D model, which is exported separately.

### 4.2 Detection Using Imaging Modules

As shown in Figure 6a, we built two hardware modules that fulfill the requirements of the fluorescence imaging principles explained in Section 3.2.

<sup>1</sup><https://ultimaker.com/software/ultimaker-cura>

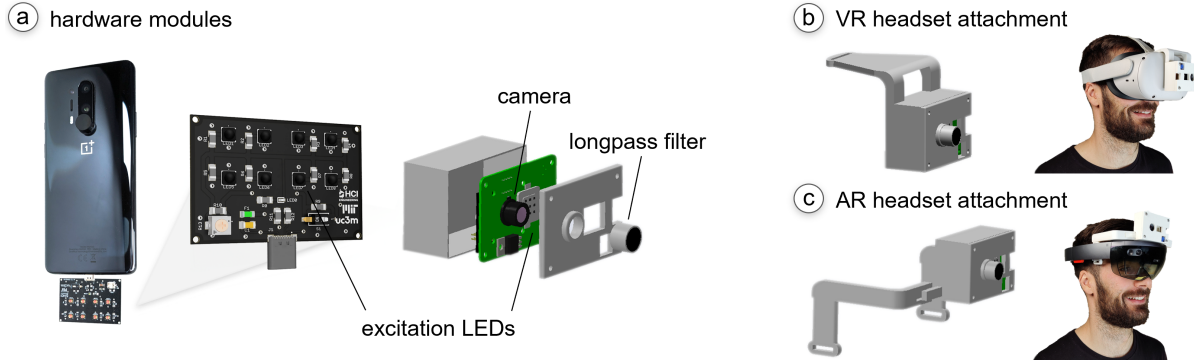


**Figure 6: Hardware modules for tracking *BrightMarkers*.**

**Smartphone attachment:** The module can be directly plugged into existing phones using a USB-C connection. It includes eight LEDs that correspond to the excitation wavelength of our filament. To ensure objects fit in the phone's field of view, half of the LEDs have a viewing angle of  $60^\circ$  and the other half  $120^\circ$  (*Stanley FWR1107MS-TR* and *FWR1108MS-TR*, \$2.5 each). The attachment weighs 47 grams, and consumes 1.6W during operation. We use it with a *OnePlus 8 Pro* that comes with an embedded NIR camera (*GalaxyCore GC5035<sup>2</sup>*), which we coupled with the appropriate longpass filter for fluorescence (*MaxMax*, \$30).

**Stand-alone module:** The module is built for high-speed fluorescence imaging and can be attached to existing AR/VR headsets. It consists of a 60-fps NIR camera (*ArduCam* with *OV2311<sup>3</sup>*, \$98) coupled with the above-mentioned longpass filter, a 10W LED grid (*Nagalugu*, \$18), and a small battery (generic 9V, \$2). A custom PCB utilizes a pulse-width modulated (PWM) signal to deliver battery power to the LEDs. It uses a timer IC (LM555) and an n-channel MOSFET to modulate the LED power via a constant current regulator (LM317), which can be adjusted using a potentiometer. In total, the module costs \$148 and weighs 118g. For prototyping purposes, we did not include a processing component on the module itself but connected its camera to an external computer using a cable. In the future, the module can be augmented with a small microprocessor to run the compute on-the-go, considering that our approach does not use compute-heavy ML models.

To be able to attach and detach the stand-alone module to existing AR/VR headsets, we designed and 3D printed an enclosure that encompasses all the parts. Figure 6b,c shows how the module is mounted on the headsets.

### 4.3 Image Processing for Marker Detection

We developed an image processing pipeline to detect the markers in real time. The process of *tracking* and *decoding* the markers is shown in Figure 7, and is explained below.

**Tracking the marker:** To keep the detection script as lightweight as possible for fast tracking, we intend to apply a small number of processing steps on the main image frame when localizing the

markers. Thus, the grayscale input image is simply binarized using Otsu's thresholding method. The binarization results in multiple identified contours. We then approximate each contour as a polygon. The polygons with four sides are our target markers (Figure 7b).

This approach keeps track of all markers irrespective of the data encoded in them (i.e., ID/string). This keeps the detection lightweight if the encoded data is not relevant to the application, e.g., when all markers are known to have the same ID.

**Decoding the marker:** For data-relevant applications, the second part of the pipeline, marker decoding, is enabled. In this part, we use each marker's bounding box from the previous step to crop out a smaller patch from the original frame (Figure 7c). While cropping, we add a small padding around the marker, i.e., 1/8 of the detected bounding box length. We then resize the patch to a certain size, i.e., 50px height. We invert the image such that the markers are dark to follow the ArUco convention. We apply a Gaussian blur to remove the noise, and apply an adaptive threshold with a block size of 15. Next, we use the ArUco detection library to decode the marker ID from the binarized patch.

The patch resizing in this part ensures that the applied block size is appropriate regardless of marker location and distance. To

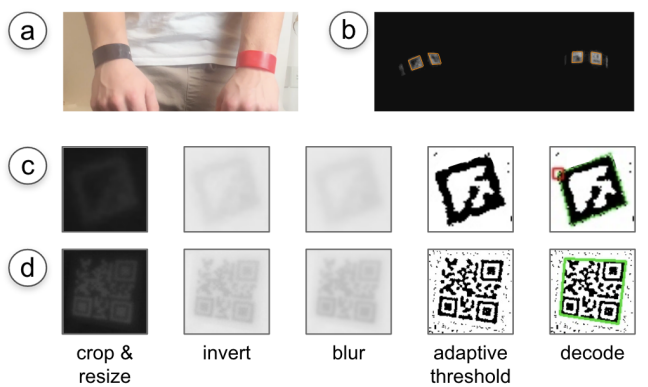


**Figure 7: *BrightMarker*'s image processing pipeline.** (a) The objects are tracked using (b) the outlines in the IR capture. (c, d) The localized markers are decoded using a set of filters.

<sup>2</sup><https://en.gcoreinc.com/products/index?cid=2&subcid=5>

<sup>3</sup><https://www.ovt.com/products/ov2311/>

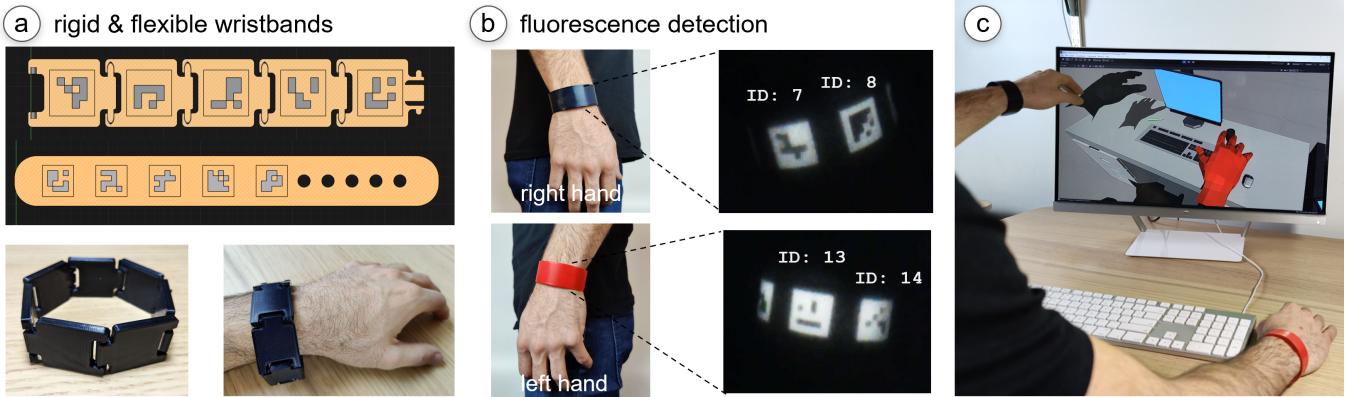


**Figure 8: Wearable for hand tracking. (a) Rigid and flexible bracelet designs with embedded markers. (b) Fluorescence imaging is used to detect the unique tracking IDs. (c) The user’s motion is digitized.**

determine this, we applied different filtering operations to a test recording consisting of 600 frames, where the marker is moved constantly (distance: 10–80cm). When the adaptive threshold was applied to an uncropped frame, the markers could be decoded from only 85.2% of the frames. On the other hand, applying the threshold after cropping and resizing allows 98.2% of the frames to be decoded.

If no ArUco marker is found in the patch, the script checks if there is a QR code or a Data Matrix. For this, we follow the same steps, except for two differences: Because the codes have more bits than ArUcos, we use a rescaling height of 100px and an adaptive threshold block size of 9. We then use a standard library to decode the codes. An example is shown in Figure 7d.

If an ArUco or a QR code is found in the patch, the script records its data and corners in an array.

*Tracking decoded markers across frames:* We also added a "caching" feature to our detection pipeline that helps track of marker data across frames, without having to run the decoding script in every new frame. When caching is enabled, we attempt to match the newly localized markers to already decoded markers from the prior frame by comparing their corner coordinates. If a new marker is found to be similar to a previous marker, we retrieve the marker data from the previous frame. Otherwise, we run the remaining decoding script. This is especially useful for QR codes, which traditionally take several frames to be *decoded*, whereas the fluorescent outline can already be *tracked* in all frames. However, to be conservative, we did not enable this feature during our evaluations (Section 6).

**Implementation:** We use *OpenCV* [6] for the implementation of our system and the *Dynamsoft*<sup>4</sup> library for the detection of the 2D barcodes (i.e., QR, Micro QR, and Data Matrix). For rapid prototyping purposes, we ran the detection script on our laptop during the development of this project. The processing of a single 640x360px frame takes 3.7 ms on average, corresponding to a 270fps on a 2020 *MacBook Pro* with a 2GHz Quad-Core *Intel Core i5* processor. Since our high-speed camera has a limit of 60fps, the detection in our applications was constrained to this rate, but our software pipeline can support higher rates as well. In our AR/VR applications, after

running *OpenCV*'s ArUco pose estimation, we use *Unity*'s coordinate transform features to convert the marker's location to a common local coordinate frame.

## 5 APPLICATIONS

In this section, we show several applications of *BrightMarker*, in which the tracking of object locations is an integral part of a process.

### 5.1 Rapid Product Tracking

Because *BrightMarkers* can localize and track embedded objects, it can be used for industrial or commercial applications in which items need to be processed in a swift manner. This can be especially useful for product and packaging logging where, although the external labels may be intentionally or unintentionally removed, it is still crucial to keep track of the item origin and other supply chain or inventory-related data.

*Tracing products on conveyor belts:* In manufacturing and packaging industries, fluorescent markers could be integrated to enable product or part tracing as part of assembly lines (Figure 1a).

*On-the-fly inventory logging:* Users can use the smartphone attachment described in Section 4.2 to activate the fluorescence of *BrightMarker*, and scan a batch of products by moving the phone to quickly capture all codes.

We note that currently, our approach is more suitable for products that are already being 3D printed (e.g. shoes [61]), and could be extended to those that will be printed in the future.

### 5.2 Wearables for Tracking Human Motion

One of the applications of *BrightMarker* is 3D printing custom wearables for tracking human motion. Figure 8a shows rigid and flexible wristbands printed with embedded markers. Embedding unique markers allows us to digitize the user's motion and distinguish between right and left hands (Figure 8b). In our setup, the detection module is mounted above the user's desk (Figure 8c).

Such tracking wearables can allow various use cases unobtrusively, such as creating digital twins and animations, increasing

<sup>4</sup><https://www.dynamsoft.com/>

safety in human-machine collaborations, posture correction warnings, or device control. Compared to existing tracking methods, the use of *BrightMarker* preserves the user's privacy since the camera only captures the marker, not the user's face or environment. Furthermore, current methods, especially those based on machine learning, are usually tuned for able-bodied people's hands. Wearables with *BrightMarker* could support applications for people with limb differences or hand impairments. In our current implementation, we produced the black wristband using PLA and the red one using ABS. Both wristbands have a small thickness, thus allowing them to be bent. In the future, more custom wearables could be printed using more flexible materials such as TPU or by utilizing FDM-based textile fabrication methods [19, 60].

### 5.3 Tangible Interfaces for MR Experiences

*BrightMarkers* can be embedded into objects to turn them into tangibles with more precise tracking capabilities for mixed reality (MR) [9]. For instance, opportunistic tangible interfaces could enhance AR interactions [15], or serve as haptic placeholders in VR.

*Appropriating physical parts as precise AR input tools:* Figure 1c shows a loudspeaker that has been unused in an office. The user wants to make use of the unplugged speaker by transforming it into a passive tangible interface for controlling the volume and bass of his AR glasses. This allows him to have a more natural and tangible input method, while touching small buttons on the glasses can be cumbersome.

*BrightMarker* has the benefit that the marker objects also include the part's identifier, i.e., the top and bottom knobs can be distinguished and assigned unique functionalities. Further, since the knobs have a uniform color and shape, it would be difficult to precisely track their rotation without the embedded *BrightMarkers*.

*Real-life objects as VR haptic props:* *BrightMarker* allows users to make use of the physical shape of existing real-world objects (e.g., toys, gadgets, sports gear) as haptic proxies in VR. For example, a "lightsaber" toy could come with integrated *BrightMarkers*, so it can be used as a different object in games. As shown in Figure 9, the lightsaber's hilt is used as a haptic placeholder for a sword to slice fruits in a game.



Figure 9: Using a lightsaber as a prop to slice fruits in a game.

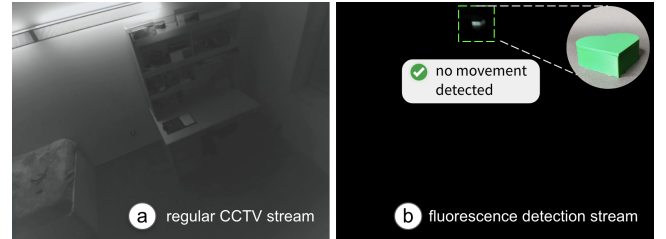


Figure 10: Privacy-preserving night vision. (a) Regular CCTVs help monitor important objects but may intrude on users' privacy. (b) Our detection setup allows tracking of solely the fluorescent objects.

### 5.4 Privacy-Preserving Night Vision

Traditional security cameras use infrared LEDs to monitor environments at night. However, these cameras might not be optimal for use in private environments, such as one's bedroom, although users may still want an alternative method to ensure the security of their valuable belongings. *BrightMarker*'s imaging system removes all details in the camera stream except for the marked objects. In Figure 10, a box that stores valuables was tagged with a *BrightMarker*, and the rest of the object surface was uniformly inlaid with the fluorescent filament so it can be captured from afar. The camera detects the shiny outline of the object, it triggers an alarm. While doing this, it preserves the user's privacy. This fluorescence-based monitoring approach could be enabled by modifying existing home security cameras, i.e., by attaching the appropriate filter on the camera and an IR source next to it as described in Section 3.2.

## 6 EVALUATION

In this section, we evaluate our system's performance under a variety of conditions, including detection distance, illumination, shell color, and speed.

### 6.1 Detection Distance, Excitation Intensity, and Surface Color

Because the embedded filament fluoresces more when exposed to a greater amount of IR excitation, the maximum distance at which a marker can be detected depends on the amount of excitation it receives. To evaluate how the IR intensity affects detection, we conducted an experiment determining the minimum amount of IR required to track vs. decode markers at varying distances from the camera. We consider tracking to be when the program finds the bounds of the *BrightMarker*; in contrast, decoding occurs when it is also able to extract the *data* of the marker (Section 4.3).

*Procedure:* We printed three square *BrightMarkers* with a 4x4 ArUco pattern of size 1"x1" (2.54cm x 2.54cm). Each *BrightMarker* was printed using shell material of a different color (blue ABS, red ABS, and black IR-PLA). We picked these to represent the variety in materials and fluorescence strength. We placed a 220cm tape measure along a table in a dark room (3lux ambient light). The NIR camera was aligned at the 0cm mark. As a baseline, we also recorded the maximum distance that a (visible) paper ArUco marker

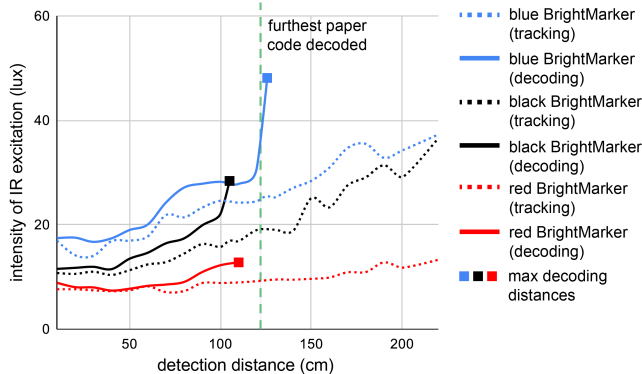


**Figure 11: Excitation intensity required with increasing marker distance from the detection setup.**

of the same size could be decoded using solely the off-the-shelf ArUco detection library.

For each trial, we started by placing a *BrightMarker* 10cm away from the camera. Then, we moved the excitation light as far away from the marker as possible until the marker is just able to be tracked. Keeping the light at this position, we measured the amount of illumination reaching the marker surface using a *Tacklife LM01* digital luxmeter. We then repeated this, but for the amount of illumination required for decoding rather than tracking. The minimum illumination needed to track and to decode the *BrightMarker* was recorded for each interval of 10cm until 220cm.

Since different shell colors allow for varying levels of fluorescence, we conducted trials for the different color prints. The chosen colors represent a wider range of fluorescence, including those which only allow minimal fluorescence (e.g., blue) and those with substantial fluorescence (e.g., red). We repeated the procedure three times for each color and plotted the average results in Figure 11.

*Results:* The tracking and decoding results are plotted separately for each color in Figure 11. The dashed lines represent the intensity needed to *track* the marker at each distance. The solid lines, however, represent the intensity to *decode* the marker at each distance.

As a baseline, the dashed green line shows the maximum distance at which a standard paper marker can be tracked and decoded (i.e., 122cm). We found that since the NIR capture filters out wavelengths lower than the *BrightMarker* emission, markers are able to be tracked at distances far greater than a paper marker. On the other hand, *BrightMarker* decoding distances were not expected to exceed this value, but were expected to be relatively close to it. While the red and black samples exhibited this behavior, the blue sample exceeded the expectation and could be decoded just past the point where a paper code can be detected. We believe this is because the filtered capture allows the decoding algorithm to ignore the noise that is in the unfiltered capture; thus, allowing it to decode the marker at a further distance. However, this does not occur for other colors because unlike blue, which allows lower levels of fluorescence, the emitted light in the red and black markers slightly bleed into the shell of the markers.

The plots also indicate a correlation between material color and the intensity of light required for detection. Overall, lower curves

indicate easier detection than higher curves, since a low curve in this plot means that less light is needed given a marker distance. The more fluorescence that the shell lets through, the less excitation is required to detect the marker, e.g., less light is required for red prints than blue prints. This is expected since the NIR camera is capturing the emitted light, so the materials that allow for more emission require less overall excitation. For this reason, we recommend using shell materials such as red ABS for tracking from far distances using weaker excitation sources.

## 6.2 Detection Rate and Marker Speed

Because the fluorescence of *BrightMarkers* is imaged using a long-pass filter, our detection setup eliminates non-marker elements from the scene, thus reducing the chance of undetected frames. We conducted an experiment to compare how the fluorescence-based detection approach improves the detection rate compared to regular *InfraredTags* [13] as the tags are being moved.

*Procedure:* We printed a red and blue *BrightMarker* with a 4x4 ArUco pattern (size: 2.54cm x 2.54cm) to represent high and low fluorescence. We then used the printer as a CNC tool: We attached each marker separately on the printhead of an *Ultimaker 3*, and placed our detection module on the printbed, with its camera looking upward at the marker. We moved the printhead in an upward conical helix trajectory to cover the remaining printer volume (21.6x21.6x130cm), while also staying in the camera's field of view. We repeated this for 12 different head speeds (range: 20mm/s - 240mm/s). We computed the detection rate throughout the trajectory from the resulting 60-fps videos.

*Results:* Across the 12 speed values, the *InfraredTag* could be tracked and decoded in only 60.73% of the frames on average ( $\text{std}=2.26$ ). For *BrightMarkers*, the red and blue sample could be *tracked* in 100% of the frames. The red sample could be *decoded* in 99.41% of the frames ( $\text{std}=0.48$ ) and the blue sample 99.83% ( $\text{std}=0.19$ ). The small standard deviation values across the different speeds show that the high-speed camera employed in our imaging module successfully avoids motion blur due to its global shutter (Section 3.2).

## 6.3 Marker Size

To test what the smallest detectable *BrightMarker* size is, we printed samples in 1mm dimension increments (range: 5-10mm) separately for red and blue ABS surface materials. For both colors, the smallest decodable marker was 6mm wide. However, the camera had to be 2cm close to the blue marker to decode it, while the red marker could be decoded from as far as 7cm. This is likely due to the higher IR absorbance of the blue shell material.

## 7 DISCUSSION

In this section, we discuss the limitations of *BrightMarker* and potential directions for future research.

### 7.1 Concentration of Fluorescent Dye

The concentration of the fluorescent dye used in the filament of *BrightMarkers* is an important factor in its detectability.

To test how the dye concentration affects the marker intensity, we obtained two small test plates from the filament manufacturer,

since a high-concentration filament is not readily available yet. Each plate was doped with fluorochrome, one with the same concentration as our filament, and another one with eight times the standard concentration. Given the same level of excitation, we measured the intensity of the emitted light when the plates are uncovered. We repeated this after covering both samples with a 1.2mm sheet made from regular red ABS filament, mimicking BrightMarker's  $t_{shell}$ .

In the uncovered comparison, we observed that the highly doped sample resulted in 33% more IR intensity than the regular sample. In the covered comparison, which represents the conditions for BrightMarker, the intensity of the highly doped sample was 20% higher than the regular sample. Thus, to further increase detection performance, further research and optimization could lead to the production of filaments with higher fluorochrome concentrations.

## 7.2 Mass Production

In the future, the BrightMarker approach may be adapted for mass-market manufacturing. For instance, instead of 3D printing, plastic overmolding could be utilized to include fluorescent materials in mass-manufactured products without any post-processing steps.

## 7.3 NIR Power

While the LED component we used in the AR/VR attachment module (Section 4.2) is rated 10W, we did not use it at full power for the headset. The potentiometer in the PCB allows us to adjust the power from 1.8W up to 3.5W. At the lowest power, a black IR PLA-covered sample can be tracked from up to 50cm away. At max power, it can be tracked at 90cm away. While, as far as we know, there are no longitudinal studies yet on NIR and eye safety, commonly used examples of NIR light include *iPhone FaceID*, *Microsoft Kinect*, and *Intel RealSense* depth cameras. For instance, RealSense D400's IR projector [27] can consume up to 4.25W.

## 7.4 Embedding Circular Markers

In this project, we embedded ArUco markers for tracking purposes. Another way to add trackers would be to use the fluorescent filament insert small circular markers, similar to OptiTrack's retro-reflective beads, underneath the object surface. Such triangulation-based tracking systems are typically deemed more robust than square marker-based methods. However, since triangulation-based methods require multiple cameras to be set up, a costly and cumbersome process, we chose to use ArUco markers for their simplicity which suits our everyday applications. Interested researchers can use our embedded fabrication approach for other tracking methods based on their needs and constraints. In the future, this could also be used to improve detection for more intricate objects, i.e., those with high-frequency surface details that would lead to local occlusion of the markers based on the viewing angle.

## 7.5 Occlusion

Object occlusion is a typical problem for most tracking methods. Similarly, BrightMarker could be occluded by the user's hands and other objects. One way to overcome this is to couple the optical tracking with magnetic tracking methods (i.e., hybrid tracking) [58]. A magnetic material could be embedded in the printed object using magnetic filaments, which would enhance the tracking when the

object is occluded by utilizing magnetic sensors. Another possible solution is to use CNN-based machine learning methods [10, 14] to recover or estimate occluded marker corners.

## 8 CONCLUSION

In this paper, we presented BrightMarker, a novel method for embedding and tracking hidden high-contrast markers using fluorescent 3D printing filaments. Our approach offers an easy-to-use solution for marker-based tracking without affecting the object's look or shape. We showed that BrightMarkers can be embedded in various object colors, and can be easily localized using a light source and camera filter that match the fluorescence characteristics of the material. Our CAD tool allows users to add markers to their 3D models before printing, and our optical detection hardware can be attached to existing AR/VR headsets for marker tracking. BrightMarker's image processing pipeline uses the captured images to robustly localize the markers. Our code and tools can be found on our website<sup>5</sup>, which we hope will widen the toolkit for the fabrication community.

Our applications demonstrate rapid product tracking, custom-fabricated wearables, tangible interfaces in AR/VR, and privacy-preserving night vision. Our evaluation shows that markers of different colors can be detected from afar and at various object speeds. We believe that our work demonstrates the potential of using fluorescence as an effective and versatile method for embedding invisible markers, and we hope it fosters further exploration and innovation in this area by the HCI and fabrication community.

## ACKNOWLEDGMENTS

We extend our sincere appreciation to *DIC Corporation* and Kyouichi Toyomura from its Composite Material Marketing Group for providing us with the fluorescent material. We are deeply grateful to the anonymous reviewers for their valuable insights and constructive feedback. Special thanks go to Eduardo López-Fraguas for his recommendations on the LED selection. We would also like to express our heartfelt thanks to Marwa AlAlawi and Ticha Sethapakdi for their meticulous proofreading and thoughtful suggestions.

## REFERENCES

- [1] 3dk.berlin. 2021. PLA Filament IR-Black. <https://3dk.berlin/en/special/115-pla-filament-ir-black.html>
- [2] Ananta Narayanan Balaji, Clayton Kimber, David Li, Shengzhi Wu, Ruofei Du, and David Kim. 2023. RetroSphere: Self-Contained Passive 3D Controller Tracking for Augmented Reality. *Proceedings of the ACM on Interactive, Mobile, Wearable and Ubiquitous Technologies* 6, 4 (Jan. 2023), 157:1–157:36. <https://doi.org/10.1145/3569479>
- [3] P. Bijl, J.J. Koenderink, and A. Toet. 1989. Visibility of blobs with a gaussian luminance profile. *Vision Research* 29, 4 (Jan. 1989), 447–456. [https://doi.org/10.1016/0042-6989\(89\)90008-4](https://doi.org/10.1016/0042-6989(89)90008-4)
- [4] Tami C. Bond and Robert W. Bergstrom. 2006. Light Absorption by Carbonaceous Particles: An Investigative Review. *Aerosol Science and Technology* 40, 1 (Jan. 2006), 27–67. <https://doi.org/10.1080/02786820500421521>
- [5] Miguel Borges, Andrew Symington, Brian Coltin, Trey Smith, and Rodrigo Ventura. 2018. HTC Vive: Analysis and Accuracy Improvement. In *2018 IEEE/RSJ International Conference on Intelligent Robots and Systems (IROS)*. 2610–2615. <https://doi.org/10.1109/IROS.2018.8593707> ISSN: 2153-0866.
- [6] Gary Bradski. 2000. The OpenCV Library. *Dr. Dobb's Journal of Software Tools* (2000).
- [7] Chris Bregler. 2007. Motion Capture Technology for Entertainment [In the Spotlight]. *IEEE Signal Processing Magazine* 24, 6 (Nov. 2007), 160–158. <https://doi.org/10.1109/MSP.2007.906023>

<sup>5</sup><https://hcie.csail.mit.edu/research/brightmarker/brightmarker.html>

- [8] DIC Corporation. 2023. DIC Global. <https://www.dic-global.com/en/>
- [9] Mustafa Doga Dogan, Patrick Baudisch, Hrvoje Benko, Michael Nebeling, Huaishu Peng, Valkyrie Savage, and Stefanie Mueller. 2022. Fabricate It or Render It? Digital Fabrication vs. Virtual Reality for Creating Objects Instantly. In *Extended Abstracts of the 2022 CHI Conference on Human Factors in Computing Systems*. Association for Computing Machinery, 5. <https://doi.org/10.1145/3491101.3516510>
- [10] Mustafa Doga Dogan, Steven Vidal Acevedo Colon, Varnika Sinha, Kaan Akşit, and Stefanie Mueller. 2021. SensiCut: Material-Aware Laser Cutting Using Speckle Sensing and Deep Learning. In *Proceedings of the 34th Annual ACM Symposium on User Interface Software and Technology*. ACM, Virtual Event USA, 15. <https://doi.org/10.1145/3472749.3474733>
- [11] Mustafa Doga Dogan, Faraz Faruqi, Andrew Day Churchill, Kenneth Friedman, Leon Cheng, Sriram Subramanian, and Stefanie Mueller. 2020. G-ID: Identifying 3D Prints Using Slicing Parameters. In *Proceedings of the 2020 CHI Conference on Human Factors in Computing Systems (CHI '20)*. Association for Computing Machinery, New York, NY, USA, 1–13. <https://doi.org/10.1145/3313831.3376202>
- [12] Mustafa Doga Dogan, Alexa F. Siu, Jennifer Healey, Curtis Wigington, Chang Xiao, and Tong Sun. 2023. StandARone: Infrared-Watermarked Documents as Portable Containers of AR Interaction and Personalization. In *Extended Abstracts of the 2023 CHI Conference on Human Factors in Computing Systems (CHI EA '23)*. Association for Computing Machinery, New York, NY, USA, 1–7. <https://doi.org/10.1145/3544549.3585905>
- [13] Mustafa Doga Dogan, Ahmad Taka, Michael Lu, Yunyi Zhu, Akshat Kumar, Aakar Gupta, and Stefanie Mueller. 2022. InfraredTags: Embedding Invisible AR Markers and Barcodes Using Low-Cost, Infrared-Based 3D Printing and Imaging Tools. In *Proceedings of the 2022 CHI Conference on Human Factors in Computing Systems*. Association for Computing Machinery, New Orleans LA USA, 9. <https://doi.org/10.1145/3491102.3501951>
- [14] Mustafa Doga Dogan, Veerapat Yotamornsunthorn, Ahmad Taka, Yunyi Zhu, Aakar Gupta, and Stefanie Mueller. 2022. Demonstrating InfraredTags: Decoding Invisible 3D Printed Tags with Convolutional Neural Networks. In *Extended Abstracts of the 2022 CHI Conference on Human Factors in Computing Systems*. Association for Computing Machinery, 7. <https://doi.org/10.1145/3491101.3519905>
- [15] Ruofei Du, Alex Olwal, Mathieu Le Goc, Shengzhi Wu, Danhang Tang, Yinda Zhang, Jun Zhang, David Joseph Tan, Federico Tombari, and David Kim. 2022. Opportunistic Interfaces for Augmented Reality: Transforming Everyday Objects into Tangible 6DoF Interfaces Using Ad hoc UI. In *CHI Conference on Human Factors in Computing Systems Extended Abstracts*. ACM, New Orleans LA USA, 1–4. <https://doi.org/10.1145/3491101.3519911>
- [16] Murat Ekici, Ahmet Çağdaş Seçkin, Ahmet Özök, and Ceyhun Karpuz. 2023. Warehouse Drone: Indoor Positioning and Product Counter with Virtual Fiducial Markers. *Drones* 7, 1 (Jan. 2023), 3. <https://doi.org/10.3390/drones7010003> Number: 1 Publisher: Multidisciplinary Digital Publishing Institute.
- [17] Martin Feick, Scott Bateman, Anthony Tang, Andre Miede, and Nicolai Marquardt. 2020. Tangi: Tangible Proxies For Embodied Object Exploration And Manipulation In Virtual Reality. In *2020 IEEE International Symposium on Mixed and Augmented Reality (ISMAR)*. IEEE, Porto de Galinhas, Brazil, 195–206. <https://doi.org/10.1109/ISMAR50242.2020.00042>
- [18] Martin Feick, Kora Persephone Regitz, Anthony Tang, and Antonio Krüger. 2022. Designing Visuo-Haptic Illusions with Proxies in Virtual Reality: Exploration of Grasp, Movement Trajectory and Object Mass. In *CHI Conference on Human Factors in Computing Systems*. ACM, New Orleans LA USA, 1–15. <https://doi.org/10.1145/3491102.3517671>
- [19] Jack Forman, Mustafa Doga Dogan, Hamilton Forsythe, and Hiroshi Ishii. 2020. DefeXtiles: 3D Printing Quasi-Woven Fabric via Under-Extrusion. In *Proceedings of the 33rd Annual ACM Symposium on User Interface Software and Technology*. ACM, Virtual Event USA, 1222–1233. <https://doi.org/10.1145/3379337.3415876>
- [20] Joshua Furtado, Hugh Liu, Gilbert Lai, Hervé Lacheray, Jason Desouza-Coelho, and Quanser. 2018. Comparative Analysis of OptiTrack Motion Capture Systems. <https://doi.org/10.25071/10315/35247>
- [21] Matteo Gastaldi, Francesca Cardano, Marco Zanetti, Guido Viscardi, Claudia Barolo, Silvia Bordiga, Shlomo Magdassi, Andrea Fin, and Ignazio Roppolo. 2021. Functional Dyes in Polymeric 3D Printing: Applications and Perspectives. *ACS Materials Letters* 3, 1 (Jan. 2021), 1–17. <https://doi.org/10.1021/acsmaterialslett.0c00455> Publisher: American Chemical Society.
- [22] Christopher Getschmann and Florian Echtler. 2021. Seedmarkers: Embeddable Markers for Physical Objects. In *Proceedings of the Fifteenth International Conference on Tangible, Embedded, and Embodied Interaction (TEI '21)*. Association for Computing Machinery, New York, NY, USA, 1–11. <https://doi.org/10.1145/3430524.3440645>
- [23] Oliver Grau and Julien Pansiot. 2012. Motion and velocity estimation of rolling shutter cameras. In *Proceedings of the 9th European Conference on Visual Media Production (CVMP '12)*. Association for Computing Machinery, New York, NY, USA, 94–98. <https://doi.org/10.1145/2414688.2414700>
- [24] George G. Guilbault (Ed.). 1990. *Practical Fluorescence* (2nd edition ed.). CRC Press, New York.
- [25] Timo Götzelmann and Daniel Schneider. 2016. CapCodes: Capacitive 3D Printable Identification and On-screen Tracking for Tangible Interaction. In *Proceedings of the 9th Nordic Conference on Human-Computer Interaction*. ACM, Gothenburg Sweden, 1–4. <https://doi.org/10.1145/2971485.2971518>
- [26] Sebastian Günther, Martin Schmitz, Florian Müller, Jan Riemann, and Max Mühlhäuser. 2017. BYO': Utilizing 3D Printed Tangible Tools for Interaction on Interactive Surfaces. In *Proceedings of the 2017 ACM Workshop on Interacting with Smart Objects*. ACM, Limassol Cyprus, 21–26. <https://doi.org/10.1145/3038450.3038456>
- [27] Intel. 2020. *RealSense Product Family D400 Series Datasheet*. Technical Report.
- [28] John Jewkes, David Sawers, and Richard Stillerman. 1969. Fluorescent Lighting. In *The Sources of Invention*, John Jewkes, David Sawers, and Richard Stillerman (Eds.), Palgrave Macmillan UK, London, 252–254. [https://doi.org/10.1007/978-1-349-00015-9\\_23](https://doi.org/10.1007/978-1-349-00015-9_23)
- [29] Han-Jong Kim, Ju-Whan Kim, and Tek-Jin Nam. 2016. miniStudio: Designers' Tool for Prototyping Ubicom Space with Interactive Miniature. In *Proceedings of the 2016 CHI Conference on Human Factors in Computing Systems*. ACM, San Jose California USA, 213–224. <https://doi.org/10.1145/2858036.2858180>
- [30] Dingzeyu Li, Avinash S Nair, Shree K Nayari, and Changxi Zheng. 2017. AirCode. *Proceedings of the 30th Annual ACM Symposium on User Interface Software and Technology - UIST '17* (2017). <https://doi.org/10.1145/3126594.3126635>
- [31] Zehua Ma, Hang Zhou, and Weiming Zhang. 2023. AnisoTag: 3D Printed Tag on 2D Surface via Reflection Anisotropy. In *Proceedings of the 2023 CHI Conference on Human Factors in Computing Systems (CHI '23)*. Association for Computing Machinery, New York, NY, USA, 1–15. <https://doi.org/10.1145/3544548.3581024>
- [32] Karola Marky, Martin Schmitz, Verena Zimmermann, Martin Herbers, Kai Kunze, and Max Mühlhäuser. 2020. 3D-Auth: Two-Factor Authentication with Personalized 3D-Printed Items. In *Proceedings of the 2020 CHI Conference on Human Factors in Computing Systems (CHI '20)*. Association for Computing Machinery, New York, NY, USA, 1–12. <https://doi.org/10.1145/3313831.3376189>
- [33] MatterHackers. 2023. Glow in the Dark PRO Series PLA Filament. <https://www.matterhackers.com/store/l/pro-series-pla/sk/MY6C8H7E>
- [34] MatterHacks. 2023. ColorFabb GlowFill Glow in the Dark Filament. <https://www.matterhackers.com/store/3d-printer-filament/colorfabb-glowfill-1.75mm>
- [35] E. Roland Menzel. 2006. Fluorescence in Forensic Science. In *Encyclopedia of Analytical Chemistry*. John Wiley & Sons, Ltd. [https://doi.org/10.1002/9780470027318.a1105\\_eprint](https://doi.org/10.1002/9780470027318.a1105_eprint) <https://onlinelibrary.wiley.com/doi/pdf/10.1002/9780470027318.a1105>
- [36] Pierre Merriaux, Yohan Dupuis, Rémi Boutteau, Pascal Vasseur, and Xavier Savatier. 2017. A Study of Vicon System Positioning Performance. *Sensors* 17 (July 2017), 1591. <https://doi.org/10.3390/s17071591>
- [37] Yamato Miyatake, Parinya Punpongsonan, Daisuke Iwai, and Kosuke Sato. 2022. interiq: Unobtrusive Edible Tags using Food 3D Printing. In *The 35th Annual ACM Symposium on User Interface Software and Technology*. ACM, Bend OR USA, 1–11. <https://doi.org/10.1145/3526113.3545669>
- [38] Leonid Naimark and Eric Foxlin. 2005. Encoded LED System for Optical Trackers. In *Proceedings of the 4th IEEE/ACM International Symposium on Mixed and Augmented Reality (ISMAR '05)*. IEEE Computer Society, USA, 150–153. <https://doi.org/10.1109/ISMAR.2005.28>
- [39] Edwin Olson. 2011. AprilTag: A robust and flexible visual fiducial system. In *2011 IEEE International Conference on Robotics and Automation*, 3400–3407. <https://doi.org/10.1109/ICRA.2011.5979561> ISSN: 1050-4729.
- [40] Parinya Punpongsonan, Daisuke Iwai, and Kosuke Sato. 2013. DeformMe: projection-based visualization of deformable surfaces using invisible textures. In *SIGGRAPH Asia 2013 Emerging Technologies (SA '13)*. Association for Computing Machinery, New York, NY, USA, 1–3. <https://doi.org/10.1145/2542284.2542292>
- [41] Francisco Romero-Ramirez, Rafael Muñoz-Salinas, and Rafael Medina-Carnicer. 2018. Speeded Up Detection of Squared Fiducial Markers. *Image and Vision Computing* 76 (June 2018). <https://doi.org/10.1016/j.imavis.2018.05.004>
- [42] Daniela K. Rosner and Kimiko Ryokai. 2010. Spyn: augmenting the creative and communicative potential of craft. In *Proceedings of the SIGCHI Conference on Human Factors in Computing Systems (CHI '10)*. Association for Computing Machinery, New York, NY, USA, 2407–2416. <https://doi.org/10.1145/1753326.1753691>
- [43] F. W. D. Rost. 1992. *Fluorescence Microscopy*. Cambridge University Press, Cambridge : New York. OCLC: 23766227.
- [44] Alberto J. Ruiz, Sadhya Garg, Samuel S. Streeter, Mia K. Giallorenzi, Ethan P. M. LaRochelle, Kimberly S. Samkoe, and Brian W. Pogue. 2021. 3D printing fluorescent material with tunable optical properties. *Scientific Reports* 11, 1 (Aug. 2021), 17135. <https://doi.org/10.1038/s41598-021-96496-0> Number: 1 Publisher: Nature Publishing Group.
- [45] Cassandra Scheirer and Chris Harrison. 2022. DynaTags: Low-Cost Fiducial Marker Mechanisms. In *Proceedings of the 2022 International Conference on Multimodal Interaction (ICMI '22)*. Association for Computing Machinery, New York, NY, USA, 432–443. <https://doi.org/10.1145/3536221.3556591>
- [46] Martin Schepers, Matteo Giuberti, and G. Bellusci. 2018. Xsens MVN: Consistent Tracking of Human Motion Using Inertial Sensing. <https://doi.org/10.13140/RG.2.222099.07205>

- [47] Frank Schieber. 2001. Modeling the Appearance of Fluorescent Colors. *Proceedings of the Human Factors and Ergonomics Society Annual Meeting* 45, 18 (Oct. 2001), 1324–1327. <https://doi.org/10.1177/154193120104501802> Publisher: SAGE Publications Inc.
- [48] Martin Schmitz, Sebastian Günther, Karola Marky, Florian Müller, Andrii Matviienko, Alexandra Voit, Roberts Marky, Max Mühlhäuser, and Thomas Kosch. 2022. Rethinking Smart Objects: The International Workshop on Interacting with Smart Objects in Interactive Spaces. In *Companion Proceedings of the 2022 Conference on Interactive Surfaces and Spaces (ISS '22)*. Association for Computing Machinery, New York, NY, USA, 64–67. <https://doi.org/10.1145/3532104.3571470>
- [49] Martin Schmitz, Martin Herbers, Niloofar Dezfouli, Sebastian Günther, and Max Mühlhäuser. 2018. Off-Line Sensing: Memorizing Interactions in Passive 3D-Printed Objects. In *Proceedings of the 2018 CHI Conference on Human Factors in Computing Systems (CHI '18)*. Association for Computing Machinery, New York, NY, USA, 1–8. <https://doi.org/10.1145/3173574.3173756>
- [50] Martin Schmitz, Mohammadreza Khalilbeigi, Matthias Balwierz, Roman Lissermann, Max Mühlhäuser, and Jürgen Steinle. 2015. Capricate: A Fabrication Pipeline to Design and 3D Print Capacitive Touch Sensors for Interactive Objects. In *Proceedings of the 28th Annual ACM Symposium on User Interface Software & Technology (UIST '15)*. Association for Computing Machinery, New York, NY, USA, 253–258. <https://doi.org/10.1145/2807442.2807503>
- [51] Martin Schmitz, Jürgen Steinle, Jochen Huber, Niloofar Dezfouli, and Max Mühlhäuser. 2017. Flexibles: Deformation-Aware 3D-Printed Tangibles for Capacitive Touchscreens. In *Proceedings of the 2017 CHI Conference on Human Factors in Computing Systems (CHI '17)*. Association for Computing Machinery, New York, NY, USA, 1001–1014. <https://doi.org/10.1145/3025453.3025663>
- [52] Dominik Schön, Thomas Kosch, Martin Schmitz, Florian Müller, Sebastian Günther, Johannes Kreutz, and Max Mühlhäuser. 2022. TrackItPipe: A Fabrication Pipeline To Incorporate Location and Rotation Tracking Into 3D Printed Objects. In *The Adjunct Publication of the 35th Annual ACM Symposium on User Interface Software and Technology*. ACM, Bend OR USA, 1–5. <https://doi.org/10.1145/3526114.3558719>
- [53] Lei Shi, Holly Lawson, Zuhao Zhang, and Shiri Azenkot. 2019. Designing Interactive 3D Printed Models with Teachers of the Visually Impaired. In *Proceedings of the 2019 CHI Conference on Human Factors in Computing Systems*. ACM, Glasgow Scotland UK, 1–14. <https://doi.org/10.1145/3290605.3300427>
- [54] Lei Shi, Ross McLachlan, Yuhang Zhao, and Shiri Azenkot. 2016. Magic Touch: Interacting with 3D Printed Graphics. In *Proceedings of the 18th International ACM SIGACCESS Conference on Computers and Accessibility (ASSETS '16)*. Association for Computing Machinery, New York, NY, USA, 329–330. <https://doi.org/10.1145/2982142.2982153>
- [55] Aleksander Sieroń, Karolina Sieroń-Stoltny, Aleksandra Kawczyk-Krupka, Wojciech Łatos, Sebastian Kwiątek, Dariusz Straszak, and Andrzej M Bugaj. 2013. The role of fluorescence diagnosis in clinical practice. *Oncotargets and therapy* 6 (July 2013), 977–982. <https://doi.org/10.2147/OTT.S42074>
- [56] Piyarat Silapasuphakornwong, Hideyuki Trii, Kazutake Uehira, and Masahiro Suzuki. 2019. Technique for Embedding Information in Objects Produced with 3D Printer Using Near Infrared Fluorescent Dye. (2019).
- [57] Subhankar Singha, Dokyoung Kim, Sankarpasad Bhuniya, and Tushar Kumeria. 2018. Fluorescence Analysis: From Sensing to Imaging. *Journal of Analytical Methods in Chemistry* 2018 (Aug. 2018), e2654127. <https://doi.org/10.1155/2018/2654127> Publisher: Hindawi.
- [58] Andrei State, Gentaro Hirota, David T. Chen, William F. Garrett, and Mark A. Livingston. 1996. Superior augmented reality registration by integrating landmark tracking and magnetic tracking. In *Proceedings of the 23rd annual conference on Computer graphics and interactive techniques - SIGGRAPH '96*. ACM Press, Not Known, 429–438. <https://doi.org/10.1145/237170.237282>
- [59] Yuta Sugiura, Diasuke Sakamoto, Anusha Withana, Masahiko Inami, and Takeo Igarashi. 2010. Cooking with robots: designing a household system working in open environments. In *Proceedings of the 28th international conference on Human factors in computing systems - CHI '10*. ACM Press, Atlanta, Georgia, USA, 2427. <https://doi.org/10.1145/175326.1753693>
- [60] Haruki Takahashi and Jeeeon Kim. 2019. 3D Printed Fabric: Techniques for Design and 3D Weaving Programmable Textiles. In *Proceedings of the 32nd Annual ACM Symposium on User Interface Software and Technology (UIST '19)*. Association for Computing Machinery, New York, NY, USA, 43–51. <https://doi.org/10.1145/3332165.3347896>
- [61] Markus Trapp, Markus Kreutz, Michael Lütjen, and Michael Freitag. 2022. Improving Sustainability of Footwear Production through 3D Printing of Shoes. 1–15. [https://doi.org/10.30844/WGAB\\_2022\\_1](https://doi.org/10.30844/WGAB_2022_1)
- [62] Gregory F. Weber and A. Sue Menko. 2005. Color image acquisition using a monochrome camera and standard fluorescence filter cubes. *BioTechniques* 38, 1 (Jan. 2005), 52–56. <https://doi.org/10.2144/05381BM06> Publisher: Future Science.
- [63] Karl D. D. Willis, Takaaki Shiratori, and Moshe Mahler. 2013. HideOut: mobile projector interaction with tangible objects and surfaces. In *Proceedings of the 7th International Conference on Tangible, Embedded and Embodied Interaction - TEI '13*. ACM Press, Barcelona, Spain, 331. <https://doi.org/10.1145/2460625.2460682>